

## Article

# Surface Oxidation of Cu<sub>2</sub>O Nanoparticles by Adsorbed Ammonia

Siwoo Lee <sup>1</sup> , Ji Won Jang <sup>2</sup> and Young Bok Ryu <sup>1,\*</sup><sup>1</sup> Korea Institute of Industrial Technology (KITECH) Ulsan Division, Ulsan 44413, Republic of Korea<sup>2</sup> Hyundai Motors, Ulsan 44259, Republic of Korea

\* Correspondence: nasug1@kitech.re.kr; Tel.: +82-52-980-6713

**Abstract:** Copper-based nanoparticles have been intensively studied owing to their superior antibacterial activity. In this study, cuprous oxide (Cu<sub>2</sub>O) nanoparticles were synthesized using two different methods. In particular, two methods for synthesizing copper oxide from NaOH, namely, with and without the addition of NH<sub>3</sub>, were used to adjust the morphology of the nanoparticles. The nanoparticles from the NH<sub>3</sub> and NaOH samples possessed an octahedral morphology. The crystal structure of the samples was confirmed by X-ray diffraction. The size distribution of the NH<sub>3</sub> sample was narrower than that of the NaOH sample. Furthermore, the average size of the NH<sub>3</sub> sample was smaller than that of the NaOH sample. Unexpectedly, the antibacterial activity of the NH<sub>3</sub> sample was found to be lower than that of the NaOH sample. X-ray photoelectron spectroscopy and Fourier-transform infrared spectroscopy revealed that the adsorbed NH<sub>3</sub> caused the surface oxidation of Cu<sub>2</sub>O nanoparticles with azide (N<sub>3</sub>) formation on surface.

**Keywords:** Cu<sub>2</sub>O nanoparticle; surface analysis; oxidation; antibacterial activity; ammonia; azide



**Citation:** Lee, S.; Jang, J.W.; Ryu, Y.B. Surface Oxidation of Cu<sub>2</sub>O Nanoparticles by Adsorbed Ammonia. *Nanomaterials* **2022**, *12*, 4242. <https://doi.org/10.3390/nano12234242>

Academic Editor: Jose L. Arias

Received: 9 November 2022

Accepted: 25 November 2022

Published: 29 November 2022

**Publisher's Note:** MDPI stays neutral with regard to jurisdictional claims in published maps and institutional affiliations.



**Copyright:** © 2022 by the authors. Licensee MDPI, Basel, Switzerland. This article is an open access article distributed under the terms and conditions of the Creative Commons Attribution (CC BY) license (<https://creativecommons.org/licenses/by/4.0/>).

## 1. Introduction

Because of the recent pandemic, wearing a mask has become a daily routine. Consequently, there have been periods when mask prices have become extremely high owing to the sold-out phenomenon, resulting in an increase in the reuse rate of masks [1]. However, although masks play a role in filtering viruses or bacteria, they do not kill bacteria or viruses. In addition, reusing masks is undesirable because the humid and warm internal conditions due to exhalation create an environment in which bacteria can thrive [2]. To prevent the growth of bacteria due to such contamination, research has been conducted to impart antibacterial activity to filter materials. Such studies have mainly involved the use of silver nanoparticles to impart antibacterial properties. Therefore, the United States Food and Drug Administration has recently begun to regulate the use of silver nanoparticles [3]. Meanwhile, the United States Environmental Protection Agency confirmed that copper and its alloys were the first metallic antimicrobial agent [4]. Thus, research on antibacterial agents that could replace silver has become active. Copper has been used for antibacterial purposes since ancient times owing to its excellent antibacterial activities. It is cheaper than silver and exists abundantly on earth; therefore, many studies on the development of antibacterial agents using copper have been conducted [5–17]. In particular, inorganic antibacterial agents are usually produced and used with nanometer size to increase the surface area. Nanoparticles are mainly synthesized using methods such as the chemical reduction method [18–22] or hydrothermal synthesis method [23,24]. Studies have been conducted to control the size and shape of particles using the chemical reduction method because the properties of nanoparticles depend on their size, shape, crystal structure, etc. [25–28]. Copper undergoes oxidation when exposed to the atmosphere [29,30]. Thus, if produced in nanoparticle form, its contact area with oxygen increases, leading to faster oxidation; this makes maintaining the antibacterial properties of copper difficult. Oxidized copper is classified into two types: cuprous oxide (Cu<sub>2</sub>O) and cupric oxide (CuO). Cu<sub>2</sub>O is superior to CuO in terms of antibacterial activity [31]. In particular, the catalytic

activity, antibacterial activity, and adsorption characteristics of Cu<sub>2</sub>O nanoparticles have been reported to be excellent when the crystal plane (111) is present on the surface of the particles [32–34]. Although mechanisms of the antibacterial activity of copper have not been clearly identified, it is generally known to be caused by direct contact between copper and bacterial cells [4,9]. Although antibacterial and adsorption properties depend on the surface properties of nanoparticles, most studies measured only the crystal information of nanoparticles through X-ray diffraction (XRD) and did not analyze the surface properties. This may cause the antibacterial activity of the synthesized Cu<sub>2</sub>O to be incorrectly analyzed. When NH<sub>3</sub> was included among materials added to control the shape of Cu<sub>2</sub>O particles, the antibacterial performance was diminished compared to the particles synthesized using other methods. The present study confirmed the reason for the decreased antibacterial properties of Cu<sub>2</sub>O octahedral nanoparticles prepared using two different methods.

## 2. Materials and Methods

The synthesis of Cu<sub>2</sub>O octahedra was performed using two methods. The first method used NH<sub>3</sub> as an additive. A difference in growth rate in the <100> direction compared to the <111> direction was generated by controlling the molar ratio of NH<sub>3</sub> and copper ions; accordingly, spherical and octahedral particles could be synthesized [32]. The <100> direction was parallel to the x-, y-, and z-axis, and the <111> directions were perpendicular to the (111) facet groups. In the other method, by increasing the amount of NaOH to be added and adsorbing an extra OH<sup>−</sup> group on the (111) crystal plane, a Cu<sub>2</sub>O octahedron with dominant crystal growth in the <100> direction could be synthesized [35].

Cu(NO<sub>3</sub>)<sub>2</sub>·3H<sub>2</sub>O (99–104%) and hydrazine hydrate (N<sub>2</sub>H<sub>4</sub>, 50–60%) reagents were purchased from Sigma-Aldrich (Merck Co., Ltd., Darmstadt, Germany). Furthermore, NaOH beads (97%) and ammonium hydroxide (25–28%) were purchased from DAEJUNG (Seoul, Korea). All materials were used without additional purification processes.

The entire Cu<sub>2</sub>O nanoparticle synthesis was performed while maintaining a temperature of 15 °C using a beaker with a double jacket and a chiller, and stirring at 300 rpm using an overhead stirrer. In the octahedral nanoparticles prepared by adding NH<sub>3</sub> (NH<sub>3</sub> sample), 4.5 mL of 14.03 M NH<sub>3</sub> was added to 180 mL of a 0.05 M solution of Cu(NO<sub>3</sub>)<sub>2</sub>·3H<sub>2</sub>O and stirred, and 18 mL of 1 M NaOH was added dropwise. The solution was stirred for 15 min, and 1.5 mL of 17.66 M N<sub>2</sub>H<sub>4</sub>, a reducing agent, was added and stirred for 90 min. In the synthesis using only NaOH (NaOH sample), 42.2 mL of 1 M NaOH was added dropwise to 360 mL of a 0.025 M Cu(NO<sub>3</sub>)<sub>2</sub>·3H<sub>2</sub>O solution and stirred for 15 min. Subsequently, 1.875 mL of 17.66 M N<sub>2</sub>H<sub>4</sub> was added and stirred for 2 h. The synthesized nanoparticles were washed 3–4 times with deionized (DI) water and ethanol and vacuum-dried.

The synthesized sample was analyzed using a scanning electron microscope (SEM, Hitachi SU820, Hitachi Co., Ltd., Tokyo, Japan) to confirm particle size and shape, and XRD (/MAX 2500-V/PC, Rigaku Co., Ltd., Tokyo, Japan) was employed to acquire a diffraction pattern using a Cu-K $\alpha$  wavelength to obtain crystal parameter values through peak analysis. Fourier-transform infrared spectroscopy (FT-IR Varian, 670, Varian Inc., CA, USA) was performed to analyze the vibration pattern of the material adsorbed on the surface. For the surface analysis of the nanoparticles, X-ray photoelectron spectroscopy (XPS, Thermo Scientific Nexsa, Thermo Fisher Scientific, Middlesex County, MA, USA) measurements were performed, and the core level shift was analyzed to obtain the information of oxidation states between Cu and O atoms. The X-ray source type used was the Microfocus monochromatic Al-K $\alpha$  (1486.6 eV) X-ray source.

To compare the antibacterial properties of the synthesized nanoparticles, the colony-forming units (CFU) of general bacteria were counted and evaluated using the dry medium film method. The antimicrobial evaluation method was as follows: first, bacteria present on the hand were collected using a pipette swab and diluted 10 from 1 to 10<sup>4</sup> times using a sterile dilution solution; then, 1 mL of the diluted solution was inoculated in each dry medium and cultured in an incubator at 37 °C for 24 h. One colony obtained from the previous culture was placed in 9 mL of buffered peptone water (BPW) solution using a

sterilized loop and subjected to primary incubation for 24 h under the same conditions as mentioned above. One milliliter of the cultured solution was placed in 9 mL of the new BPW solution and incubated for a second time for 24 h, and the second cultured solution was diluted 10 times to the power of 1–3 and incubated in a dry medium to obtain the standard bacterial solution. In the experimental group, 0.01 g of the synthesized nanoparticles was dispersed in 30 mL of DI water, mixed with a standard bacterial solution at a volume ratio of 1:1, and cultured. In the control group, DI water was added to the standard bacterial solution in the same way as in the experimental group and cultured to compare the number of CFUs.

### 3. Results and Discussion

To confirm the crystal structure and component, XRD measurement was conducted on the  $\text{Cu}_2\text{O}$  nanoparticles synthesized using the two methods. The crystal structure was confirmed using the International Center for Diffraction Data (ICDD) library.

As shown in Figure 1, the XRD pattern of the particles synthesized by adding  $\text{NH}_3$  (hereinafter,  $\text{NH}_3$  sample) matched the crystal pattern of ICDD PDF <01-071-4310>  $\text{Cu}_2\text{O}$ , and the XRD pattern of the particles synthesized by adding NaOH (hereinafter, NaOH sample) matched the crystal pattern of ICDD PDF <98-000-0186>  $\text{Cu}_2\text{O}$ ; thus, the crystal structures of both samples were confirmed. The average crystal size was obtained from the Scherrer equation using the full width at half maximum obtained through the analysis of the crystal planes of the main peaks (111) and (200) of the XRD patterns, and the d-spacing value was obtained using Bragg's law. The crystal sizes of the  $\text{NH}_3$  and NaOH samples were 19 and 25.04 nm, respectively; thus, the crystal size was larger when only NaOH was used. The size distribution of the nanoparticles verified from the SEM images shown in Figure 2 was 300–450 and 250–730 nm for  $\text{NH}_3$  and NaOH, respectively; the size distribution of the NaOH sample was wider than that of the  $\text{NH}_3$  sample.

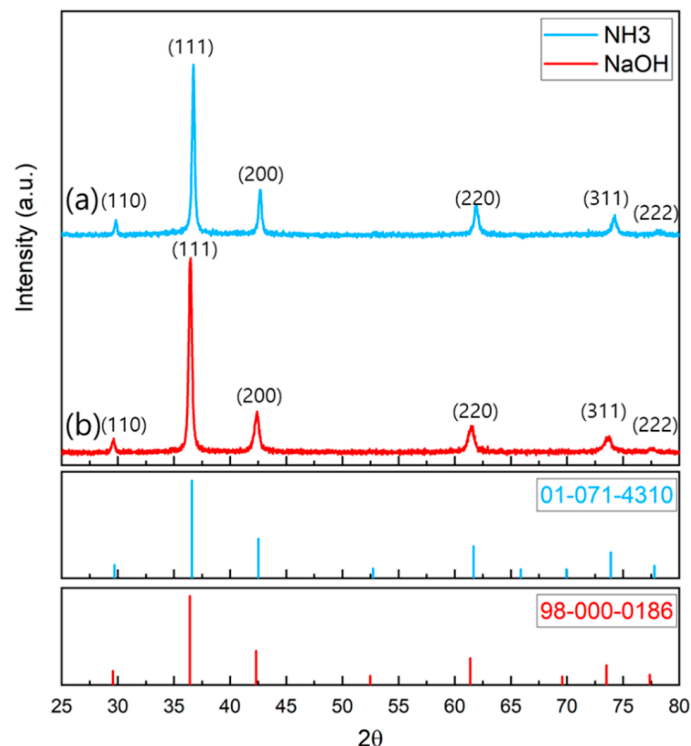


**Figure 1.** XRD patterns of  $\text{Cu}_2\text{O}$  NPs (a) with  $\text{NH}_3$  (ICDD PDF#01-071-4310) and (b) without  $\text{NH}_3$  (ICDD PDF#98-000-0186).

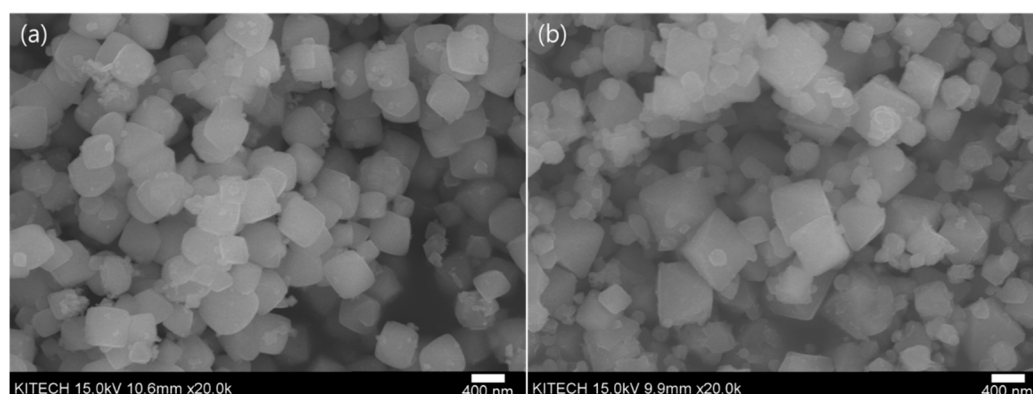


**Figure 2.** SEM images of Cu<sub>2</sub>O NPs (a) with NH<sub>3</sub> and (b) without NH<sub>3</sub>.

The antibacterial evaluation presented in Figure 3 and Table 1 reveals that an average of 706.8 colonies were formed in the control group (a) and 54.3 colonies were formed in the NaOH sample (b). By contrast, the number of colonies in the NH<sub>3</sub> sample (c) significantly increased to 466.3 compared to that in the NaOH sample. This is an unexpected result because the NaOH sample had a larger average size of nanoparticles compared with the NH<sub>3</sub> sample; thus, its antibacterial activity was expected to be worse than that of the NH<sub>3</sub> sample. When the NaOH sample was thermally treated at 80 °C, 465.5 colonies (a higher value than in the untreated sample) were obtained. The surface oxidation of the Cu<sub>2</sub>O particles was assumed to be the reason for the decreased antibacterial activity of the NH<sub>3</sub> sample.

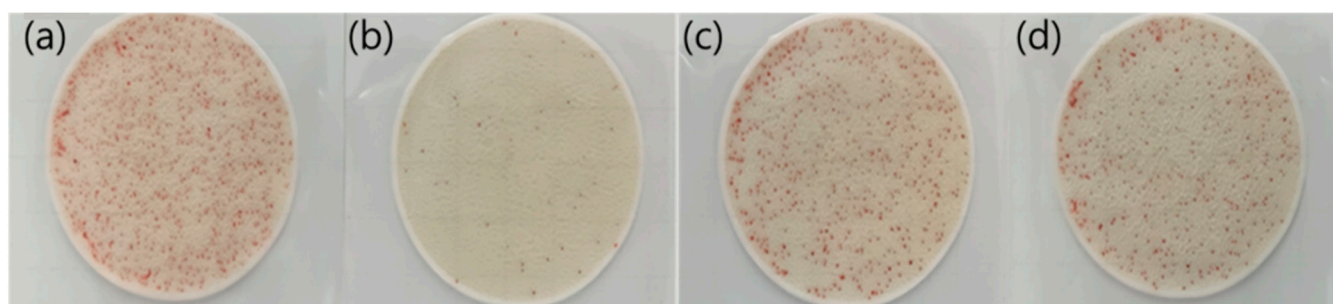


**Figure 3.** Antibacterial activity of (a) control, (b) NaOH sample (c) NH<sub>3</sub> sample, and (d) 80 °C treated NaOH sample.

**Table 1.** Average colony number of samples.

Sample	Control	NaOH	NH <sub>3</sub>	NaOH 80 °C
Colony count (average)	706.8	54.3	466.3	465.5

Figure 4 shows the FT-IR spectra of the NH<sub>3</sub> and NaOH samples. In the spectrum of the NaOH sample, Cu<sub>2</sub>O and CuO, represented by 623 cm<sup>-1</sup> [36] and 497 cm<sup>-1</sup> [37], respectively, were observed. However, in addition to the Cu<sub>2</sub>O peak at 623 cm<sup>-1</sup> and the CuO peak at 516 cm<sup>-1</sup> [38] in the spectrum of the NH<sub>3</sub> sample, a new peak appeared at 2053 cm<sup>-1</sup>, which was close to 2030 cm<sup>-1</sup>, the peak that was observed in Busca et al.'s study [39]. This peak is attributed to the azide (N<sub>3</sub>) species. In addition, a N–H stretching peak at 3317 cm<sup>-1</sup> was observed [40].

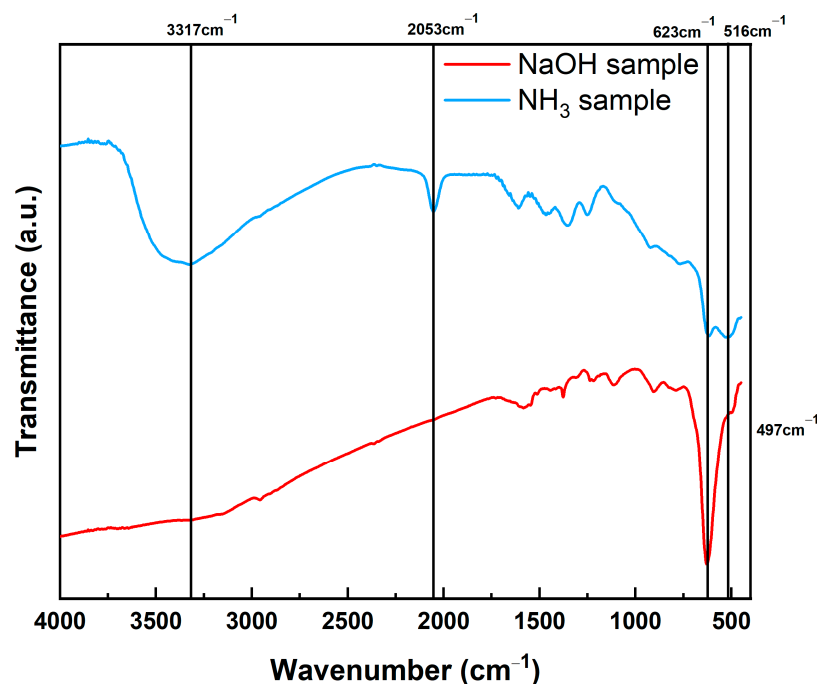


Figure 4. FT-IR spectra of the  $\text{NH}_3$  and NaOH samples.

To investigate the surface properties of the nanoparticles, XPS measurement, which could be used to analyze the surface information to a depth of 10 nm, was applied to the samples. Figure 5 shows the binding energy of the Cu  $2p_{3/2}$  region according to the presence or absence of 80 °C heat treatment of the  $\text{NH}_3$  and NaOH samples. The vacuum-dried  $\text{NH}_3$  and NaOH samples appeared as  $\text{Cu}_2\text{O}$  in the XRD pattern shown in Figure 1. However, surface analysis with XPS revealed that the  $\text{NH}_3$  sample had a strong  $\text{Cu}^{2+}$  satellite peak between 940 and 945 eV and peaks at 933.66 and 953.5 eV; thus,  $\text{CuO}$  could be inferred to exist on the surface. By contrast, the NaOH sample had a  $\text{Cu}_2\text{O}$  peak at 932.48 eV and the bonding of  $\text{Cu}_2\text{O}$  existed at 952.3 eV, indicating that the surface was  $\text{Cu}_2\text{O}$  [41].

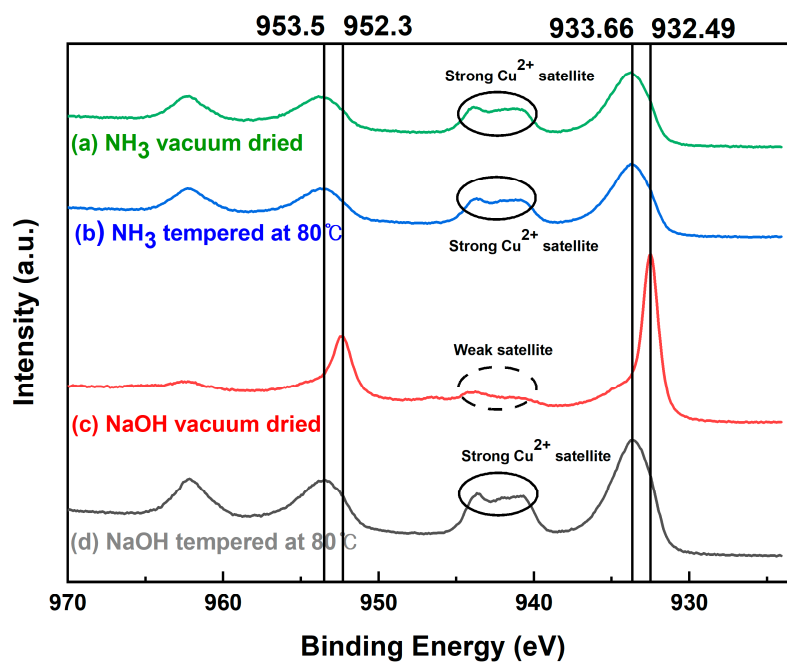


Figure 5. XPS spectra of  $\text{Cu}_2\text{O}$  NPs: (a)  $\text{NH}_3$  sample dried in vacuum, (b)  $\text{NH}_3$  sample tempered at 80 °C, (c) NaOH sample dried in vacuum, and (d) NaOH sample tempered at 80 °C.

In the case of heat-treated samples at 80 °C, the surface of both samples was oxidized, forming a CuO layer. In the crystal structure obtained from XRD measurement after thermal treatment with different temperatures to compare the oxidation stability (Figure 6), the NH<sub>3</sub> sample showed a CuO crystal phase from 200 °C, while the NaOH sample showed a CuO crystal phase after 300 °C; the thermal oxidation stability of the NaOH sample was better than that of the NH<sub>3</sub> sample. This is consistent with the preceding results from XPS, in which the surface of the NH<sub>3</sub> sample was already oxidized to form CuO.

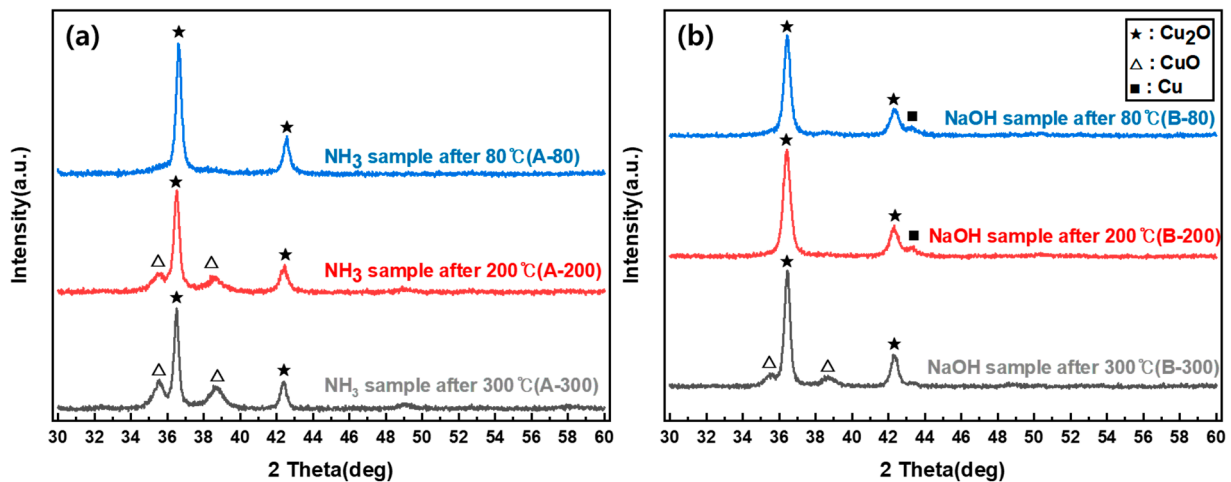


Figure 6. XRD patterns after heat treatment: (a) NH<sub>3</sub> samples; (b) NaOH samples.

As illustrated in Figure 7, the peaks related to the azide (N<sub>3</sub>) group and a wide N–H group of 3317 cm<sup>-1</sup> formed in the NH<sub>3</sub> sample decreased gradually as the heat treatment temperature increased, and all peaks disappeared after the heat treatment at 300 °C. The phenomenon in which an azide group is formed on the Cu<sub>2</sub>O surface is assumed to occur when NH<sub>3</sub> is decomposed while being adsorbed on the Cu<sub>2</sub>O surface. A previous study reported that the formation of an azide group after N<sub>2</sub>H<sub>4</sub> adsorbed on the TiO<sub>2</sub> surface was decomposed on the surface with NH<sub>3</sub> [42].

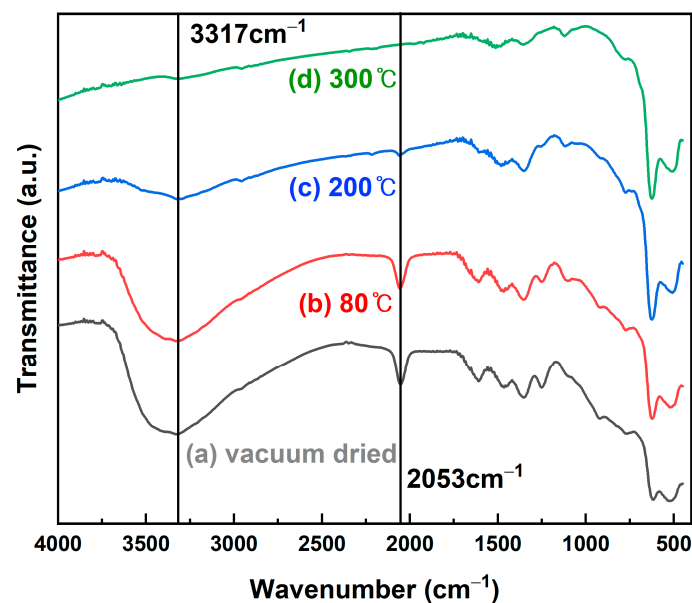


Figure 7. FT-IR spectra of NH<sub>3</sub> samples under (a) vacuum drying and heat treatment at (b) 80 °C, (c) 200 °C, and (d) 300 °C.

The CuO shell formation of Cu<sub>2</sub>O nanocrystals is considered to be similarly associated with the adsorption of NH<sub>3</sub>. Incidentally, a study reported that NO<sub>x</sub> is reduced using NH<sub>3</sub> and Cu<sub>2</sub>O catalysts [43]. Because Cu(NO<sub>3</sub>)<sub>2</sub> is used as the precursor, sufficient NO<sub>3</sub><sup>−</sup> ions are present around it. Therefore, NH<sub>3</sub> and NO<sub>3</sub><sup>−</sup> ions present on the metal surface are assumed to interact and reduce to NO<sub>2</sub>; accordingly, Cu<sub>2</sub>O is oxidized to form CuO on the surface. The result that NO<sub>3</sub><sup>−</sup> ions adsorbed on the metal surface are reduced to NO<sub>2</sub><sup>−</sup> ions has been reported [44].

When the NH<sub>3</sub> sample was heated at heat treatment temperatures of 80 °C, 200 °C, and 300 °C, the peaks of the azide group of 2053 cm<sup>−1</sup> formed on the surface gradually decreased in size as the temperature increased and disappeared at 300 °C. In addition, the N–H plane observed at 3317 cm<sup>−1</sup> disappeared equally.

#### 4. Conclusions

This study revealed that, when NH<sub>3</sub> is added in the synthesis of Cu<sub>2</sub>O nanoparticles, a CuO shell is formed on the surface of the Cu<sub>2</sub>O nanoparticles. Consequently, the antibacterial activity of the nanoparticles from the NH<sub>3</sub> sample was lower than that of the Cu<sub>2</sub>O nanoparticles prepared using only NaOH. When fabricating nanoparticles, which have important surface properties, NH<sub>3</sub> could form unwanted oxides on the surface owing to redox reactions; thus, because XRD crystal analysis cannot reveal oxides formed on the surface, surface analysis techniques such as XPS must be performed simultaneously to accurately study nanoparticle properties. For further understanding oxidation caused by NH<sub>3</sub> adsorption, using another copper precursor such as copper acetate (Cu(Ac)<sub>2</sub>) or copper chloride (CuCl<sub>2</sub>), or another reducing agent with NH<sub>3</sub> could be part of future experiments. These are currently being considered for further investigation. In addition, to investigate the effect of CuO shell on various species such as Gram-positive (pyogenes, *Strep. agalactiae*, enterococci) or Gram-negative (*Acinetobacter*, *E. coli*, *Klebsiella*) bacteria, the antibacterial activity of each species could be further examined. Although the formed CuO shell on Cu<sub>2</sub>O nanoparticles diminished the antibacterial activity, the Cu<sub>2</sub>O/CuO core-shell nanoparticles are expected to be used as photoelectrochemical catalysts owing to the charge separation for organic degradation [45,46].

**Author Contributions:** Conceptualization, S.L.; validation S.L. and J.W.J.; formal analysis, S.L. and J.W.J.; investigation, S.L. and J.W.J.; writing—original draft preparation, S.L. and J.W.J.; writing—review and editing, S.L. and Y.B.R.; visualization, J.W.J. and S.L.; supervision, Y.B.R.; project administration, Y.B.R.; funding acquisition, Y.B.R. All authors have read and agreed to the published version of the manuscript.

**Funding:** This research was conducted with the support of the Korea Institute of Industrial Technology through project “Development of fiber-based technology for reduction of hazardous substances in the air (kitech EO-22-0002)”.

**Data Availability Statement:** Not applicable.

**Conflicts of Interest:** The authors declare no conflict of interest.

#### References

1. Czubyt, M.P.; Stecy, T.; Popke, E.; Aitken, R.; Jabusch, K.; Pound, R.; Lawes, P.; Ramjiawan, B.; Pierce, G.N. N95 mask reuse in a major urban hospital: COVID-19 response process and procedure. *J. Hosp. Infect.* **2020**, *106*, 277–282. [CrossRef] [PubMed]
2. Seidi, F.; Deng, C.; Zhong, Y.; Liu, Y.; Huang, Y.; Li, C.; Xiao, H. Functionalized Masks: Powerful Materials against COVID-19 and Future Pandemics. *Small* **2021**, *17*, 2102453. [CrossRef] [PubMed]
3. U.S. Food and Drug Administration. *Nanotechnology Task Force Report 2020*; U.S. Food and Drug Administration: VA, USA, 2020. Available online: <https://www.fda.gov/media/140395/download> (accessed on 1 November 2022).
4. Vincent, M.; Duval, R.E.; Hartemann, P.; Engels-Deutsch, M. Contact killing and antimicrobial properties of copper. *J. Appl. Microbiol.* **2018**, *124*, 1032–1046. [CrossRef] [PubMed]
5. Chatterjee, A.K.; Sarkar, R.K.; Chattopadhyay, A.P.; Aich, P.; Chakraborty, R.; Basu, T. A simple robust method for synthesis of metallic copper nanoparticles of high antibacterial potency against *E. coli*. *Nanotechnology* **2012**, *23*, 085103. [CrossRef] [PubMed]
6. Jia, B.; Mei, Y.; Cheng, L.; Zhou, J.; Zhang, L. Preparation of copper nanoparticles coated cellulose films with antibacterial properties through one-step reduction. *ACS Appl. Mater. Interfaces* **2012**, *4*, 2897–2902. [CrossRef] [PubMed]

7. Longano, D.; Ditaranto, N.; Cioffi, N.; Di Niso, F.; Sibillano, T.; Ancona, A.; Conte, A.; Del Nobile, M.A.; Sabbatini, L.; Torsi, L. Analytical characterization of laser-generated copper nanoparticles for antibacterial composite food packaging. *Anal. Bioanal. Chem.* **2012**, *403*, 1179–1186. [[CrossRef](#)] [[PubMed](#)]
8. Lee, H.-J.; Song, J.Y.; Kim, B.S. Biological synthesis of copper nanoparticles using *Magnolia kobus* leaf extract and their antibacterial activity. *J. Chem. Technol. Biotechnol.* **2013**, *88*, 1971–1977. [[CrossRef](#)]
9. Chatterjee, A.K.; Chakraborty, R.; Basu, T. Mechanism of antibacterial activity of copper nanoparticles. *Nanotechnology* **2014**, *25*, 135101. [[CrossRef](#)] [[PubMed](#)]
10. Din, M.I.; Arshad, F.; Hussain, Z.; Mukhtar, M. Green Adeptness in the Synthesis and Stabilization of Copper Nanoparticles: Catalytic, Antibacterial, Cytotoxicity, and Antioxidant Activities. *Nanoscale Res. Lett.* **2017**, *12*, 638. [[CrossRef](#)] [[PubMed](#)]
11. Prabhhu, Y.T.; Venkateswara Rao, K.; Sessa Sai, V.; Pavani, T. A facile biosynthesis of copper nanoparticles: A micro-structural and antibacterial activity investigation. *J. Saudi Chem. Soc.* **2017**, *21*, 180–185. [[CrossRef](#)]
12. Rajeshkumar, S.; Menon, S.; Venkat Kumar, S.; Tambuwala, M.M.; Bakshi, H.A.; Mehta, M.; Satija, S.; Gupta, G.; Chellappan, D.K.; Thangavelu, L.; et al. Antibacterial and antioxidant potential of biosynthesized copper nanoparticles mediated through *Cissus arnotiana* plant extract. *J. Photochem. Photobiol. B Biol.* **2019**, *197*, 111531. [[CrossRef](#)] [[PubMed](#)]
13. Bastos, C.A.P.; Faria, N.; Wills, J.; Malmberg, P.; Scheers, N.; Rees, P.; Powell, J.J. Copper nanoparticles have negligible direct antibacterial impact. *NanoImpact* **2020**, *17*, 100192. [[CrossRef](#)]
14. Lv, P.; Zhu, L.; Yu, Y.; Wang, W.; Liu, G.; Lu, H. Effect of NaOH concentration on antibacterial activities of Cu nanoparticles and the antibacterial mechanism. *Mater. Sci. Eng. C* **2020**, *110*, 110669. [[CrossRef](#)] [[PubMed](#)]
15. Jayaramudu, T.; Varaprasad, K.; Pyarasani, R.D.; Reddy, K.K.; Akbari-Fakhrabadi, A.; Carrasco-Sánchez, V.; Amalraj, J. Hydroxypropyl methylcellulose-copper nanoparticle and its nanocomposite hydrogel films for antibacterial application. *Carbohydr. Polym.* **2021**, *254*, 117302. [[CrossRef](#)] [[PubMed](#)]
16. Crisan, M.C.; Teodora, M.; Lucian, M. Copper Nanoparticles: Synthesis and Characterization, Physiology, Toxicity and Antimicrobial Applications. *Appl. Sci.* **2022**, *12*, 141. [[CrossRef](#)]
17. Gonçalves, R.A.; Ku, J.W.K.; Zhang, H.; Salim, T.; Oo, G.; Zinn, A.A.; Boothroyd, C.; Tang, R.M.Y.; Gan, C.L.; Gan, Y.-H.; et al. Copper-Nanoparticle-Coated Fabrics for Rapid and Sustained Antibacterial Activity Applications. *ACS Appl. Nano Mater.* **2022**, *5*, 12876–12886. [[CrossRef](#)]
18. Sood, A.; Arora, V.; Shah, J.; Kotnala, R.K.; Jain, T.K. Ascorbic acid-mediated synthesis and characterisation of iron oxide/gold core-shell nanoparticles. *J. Exp. Nanosci.* **2015**, *11*, 370–382. [[CrossRef](#)]
19. Ong, H.R.; Rahman Khan, M.M.; Ramli, R.; Du, Y.; Xi, S.; Yunus, R.M. Facile synthesis of copper nanoparticles in glycerol at room temperature: Formation mechanism. *RSC Adv.* **2015**, *5*, 24544–24549. [[CrossRef](#)]
20. Marković, D.; Ašanin, J.; Nunney, T.; Radovanović, Ž.; Radoičić, M.; Mitrić, M.; Mišić, D.; Radetić, M. Broad Spectrum of Antimicrobial Activity of Cotton Fabric Modified with Oxalic Acid and CuO/Cu<sub>2</sub>O Nanoparticles. *Fibers Polym.* **2019**, *20*, 2317–2325. [[CrossRef](#)]
21. Tam, S.K.; Ng, K.M. High-concentration copper nanoparticles synthesis process for screen-printing conductive paste on flexible substrate. *J. Nanopart. Res.* **2015**, *17*, 466. [[CrossRef](#)]
22. Sayed, M.; Zhang, L.; Yu, J. Plasmon-induced interfacial charge-transfer transition prompts enhanced CO<sub>2</sub> photoreduction over Cu/Cu<sub>2</sub>O octahedrons. *Chem. Eng. J.* **2020**, *397*, 125390. [[CrossRef](#)]
23. Cho, C.W.; Tai, W.P.; Lee, H.S. Characteristics of Zirconia Nanoparticles with Hydrothermal Synthesis Process. *Appl. Chem. Eng.* **2014**, *25*, 564–569. [[CrossRef](#)]
24. Sōmiya, S.; Roy, R. Hydrothermal synthesis of fine oxide powders. *Bull. Mater. Sci.* **2000**, *23*, 453–460. [[CrossRef](#)]
25. Gou, L.; Murphy, C.J. Controlling the size of Cu<sub>2</sub>O nanocubes from 200 to 25 nm. *J. Mater. Chem.* **2004**, *14*, 735–738. [[CrossRef](#)]
26. Gilbertson, L.M.; Albalghiti, E.M.; Fishman, Z.S.; Perreault, F.; Corredor, C.; Posner, J.D.; Elimelech, M.; Pfefferle, L.D.; Zimmerman, J.B. Shape-Dependent Surface Reactivity and Antimicrobial Activity of Nano-Cupric Oxide. *Environ. Sci. Technol.* **2016**, *50*, 3975–3984. [[CrossRef](#)] [[PubMed](#)]
27. Xiong, L.; Yu, H.; Nie, C.; Xiao, Y.; Zeng, Q.; Wang, G.; Wang, B.; Lv, H.; Li, Q.; Chen, S. Size-controlled synthesis of Cu<sub>2</sub>O nanoparticles: Size effect on antibacterial activity and application as a photocatalyst for highly efficient H<sub>2</sub>O<sub>2</sub> evolution. *RSC Adv.* **2017**, *7*, 51822–51830. [[CrossRef](#)]
28. Jung, H.-Y.; Seo, Y.; Park, H.; Huh, Y.-D. Morphology-controlled Synthesis of Octahedral-to-Rhombic Dodecahedral Cu<sub>2</sub>O Microcrystals and Shape-dependent Antibacterial Activities. *Bull. Korean Chem. Soc.* **2015**, *36*, 1828–1833. [[CrossRef](#)]
29. Odneval, I.; Leygraf, C. Atmospheric Corrosion of Copper in a Rural Atmosphere. *J. Electrochem. Soc.* **1995**, *142*, 3682. [[CrossRef](#)]
30. FitzGerald, K.P.; Nairn, J.; Skennerton, G.; Atrens, A. Atmospheric corrosion of copper and the colour, structure and composition of natural patinas on copper. *Corros. Sci.* **2006**, *48*, 2480–2509. [[CrossRef](#)]
31. Meghana, S.; Kabra, P.; Chakraborty, S.; Padmavathy, N. Understanding the pathway of antibacterial activity of copper oxide nanoparticles. *RSC Adv.* **2015**, *5*, 12293–12299. [[CrossRef](#)]
32. Xu, H.; Wang, W.; Zhu, W. Shape Evolution and Size-Controllable Synthesis of Cu<sub>2</sub>O Octahedra and Their Morphology-Dependent Photocatalytic Properties. *J. Phys. Chem. B* **2006**, *110*, 13829–13834. [[CrossRef](#)] [[PubMed](#)]
33. Ren, J.; Wang, W.; Sun, S.; Zhang, L.; Wang, L.; Chang, J. Crystallography Facet-Dependent Antibacterial Activity: The Case of Cu<sub>2</sub>O. *Ind. Eng. Chem. Res.* **2011**, *50*, 10366–10369. [[CrossRef](#)]

34. Xu, Y.; Wang, H.; Yu, Y.; Tian, L.; Zhao, W.; Zhang, B. Cu<sub>2</sub>O Nanocrystals: Surfactant-Free Room-Temperature Morphology-Modulated Synthesis and Shape-Dependent Heterogeneous Organic Catalytic Activities. *J. Phys. Chem. C* **2011**, *115*, 15288–15296. [[CrossRef](#)]
35. Chen, K.; Xue, D. Chemoaffinity-mediated crystallization of Cu<sub>2</sub>O: A reaction effect on crystal growth and anode property. *CrystEngComm* **2013**, *15*, 1739–1746. [[CrossRef](#)]
36. Khan, M.; Ullah, M.; Iqbal, T.; Mahmood, H.; Khan, A.A.; Shafique, M.; Majid, A.; Ahmed, A.; Khan, N.A. Surfactant assisted synthesis of cuprous oxide (Cu<sub>2</sub>O) nanoparticles via solvothermal process. *Nanosci. Nanotechnol. Res.* **2015**, *3*, 16–22.
37. Ethiraj, A.S.; Kang, D.J. Synthesis and characterization of CuO nanowires by a simple wet chemical method. *Nanoscale Res. Lett.* **2012**, *7*, 70. [[CrossRef](#)] [[PubMed](#)]
38. Elango, M.; Deepa, M.; Subramanian, R.; Mohamed Musthafa, A. Synthesis, Characterization, and Antibacterial Activity of Polyindole/Ag–CuO Nanocomposites by Reflux Condensation Method. *Polym.-Plast. Technol. Eng.* **2018**, *57*, 1440–1451. [[CrossRef](#)]
39. Ramis, G.; Yi, L.; Busca, G.; Turco, M.; Kotur, E.; Willey, R.J. Adsorption, Activation, and Oxidation of Ammonia over SCR Catalysts. *J. Catal.* **1995**, *157*, 523–535. [[CrossRef](#)]
40. Chen, H.; Liu, Y.; Gong, T.; Wang, L.; Zhao, K.; Zhou, S. Use of intermolecular hydrogen bonding to synthesize triple-shape memory supermolecular composites. *RSC Adv.* **2013**, *3*, 7048–7056. [[CrossRef](#)]
41. Strohmeier, B.R.; Levdin, D.E.; Field, R.S.; Hercules, D.M. Surface spectroscopic characterization of CuAl<sub>2</sub>O<sub>3</sub> catalysts. *J. Catal.* **1985**, *94*, 514–530. [[CrossRef](#)]
42. Chuang, C.-C.; Shiu, J.-S.; Lin, J.-L. Interaction of hydrazine and ammonia with TiO<sub>2</sub>. *Phys. Chem. Chem. Phys.* **2000**, *2*, 2629–2633. [[CrossRef](#)]
43. Zhang, X.; Wang, H.; Meng, L.; Nie, X.; Qu, Z. Investigation on Cu<sub>2</sub>O Surface Reconstruction and Catalytic Performance of NH<sub>3</sub>-SCO by Experimental and DFT Studies. *ACS Appl. Energy Mater.* **2020**, *3*, 3465–3476. [[CrossRef](#)]
44. Epron, F.; Gauthard, F.; Pinéda, C.; Barbier, J. Catalytic Reduction of Nitrate and Nitrite on Pt–Cu/Al<sub>2</sub>O<sub>3</sub> Catalysts in Aqueous Solution: Role of the Interaction between Copper and Platinum in the Reaction. *J. Catal.* **2001**, *198*, 309–318. [[CrossRef](#)]
45. Han, L.; Zhan, W.; Liang, X.; Zhang, W.; Huang, R.; Chen, R.; Ni, H. In-situ generation Cu<sub>2</sub>O/CuO core-shell heterostructure based on copper oxide nanowires with enhanced visible-light photocatalytic antibacterial activity. *Ceram. Int.* **2022**, *48*, 22018–22030. [[CrossRef](#)]
46. Jiang, D.; Xue, J.; Wu, L.; Zhou, W.; Zhang, Y.; Li, X. Photocatalytic performance enhancement of CuO/Cu<sub>2</sub>O heterostructures for photodegradation of organic dyes: Effects of CuO morphology. *Appl. Catal. B Environ.* **2017**, *211*, 199–204. [[CrossRef](#)]